PHYSICAL REVIEW B, VOLUME 65, 195408

Growth mode of epitaxial superlattices $[\mathrm{BaCuO}_{2+x}]_2/[\mathrm{CaCuO}_2]_3$ on vicinal (001) SrTiO_3 substrates studied by x-ray diffraction

C. Aruta*
INFM-Dipartimento Scienze e Tecnologie Fisiche ed Energetiche, Università di Roma "Tor Vergata,"
Via di Tor Vergata 110, I-00133 Roma, Italy

F. Ricci†
INFM-Dipartimento di Scienze Fisiche, Universita' di Napoli "Federico II," Piazzale Tecchio 80, I-80125 Napoli, Italy

G. Balestrino, S. Lavanga, P. G. Medaglia, P. Orgiani, and A. Tebano
INFM-Dipartimento Scienze e Tecnologie Fisiche ed Energetiche, Università di Roma "Tor Vergata,"
Via di Tor Vergata 110, I-00133 Roma, Italy

J. Zegenhagen
European Synchrotron Radiation Facility, B.P. 220, F-38043 Grenoble Cedex, France

(Received 30 October 2001; revised manuscript received 30 January 2002; published 22 April 2002)

Structural and morphological properties of $[\mathrm{BaCuO}_{2+x}]_2/[\mathrm{CaCuO}_2]_3$ superlattices with different thicknesses, grown on specially prepared vicinal (001) SrTiO_3 substrates, are investigated. Using undulator radiation from a third-generation synchrotron we have performed x-ray-diffraction and diffuse scattering measurements, both in conventional and grazing-incidence geometries. We obtain detailed information about the role of the miscut of the substrate on the growth process of these superlattices. The critical thickness for pseudomorphic growth is found to depend on the miscut angle and, to a lesser extent on the film thickness. Thus the miscut of the substrate surprisingly influences the phase transition from the pseudomorphic, pseudotetragonal state to the orthorhombic state. Our results show that the interface morphology depends on the specific miscut of the substrate. Isotropic ripples, anisotropic ripples, and a fractal structure are formed upon slightly increasing the miscut angle from about 0.15° up to angles less than 1°. The ripples accompany the two-dimensional, layer-by-layer growth mode, which prevails for thin layers of the superlattices on well-oriented surfaces.

DOI: 10.1103/PhysRevB.65.195408 PACS number(s): 68.35.Ct, 74.80.Dm, 81.15.Fg

I. INTRODUCTION

The challenge of integrating complex oxide materials into heterostructures and multilayers with interesting functional properties, such as superconducting,[1–3] magnetic,[4–6] and dielectric properties,[7,8] has stimulated the development of layer-by-layer epitaxial growth techniques. Nevertheless, the growth of oxide thin films is not yet well enough established, because of the particular features related to their complex, often anisotropic structure, with a relatively large number of chemical elements.[9–11] However, understanding the growth process, and consequently being able to control the interface morphology and microstructure, is of fundamental interest and importance for the fabrication of devices made of these materials.

Employing vicinal substrates for the growth of thin films is a well-known technique to control or improve interface and surface properties. Vicinal substrates were, in fact, systematically employed to study the growth process of high-temperature superconducting materials (HTS's),[12–14] and to control the structural defects, thereby influencing the transport properties at those compounds.[15–18] Moreover, even substrate surfaces, which are nominally oriented exactly, may have miscut angles, which can influence the structure and the defect ordering in the film, leading to anisotropic properties even for an otherwise isotropic material. We have already observed this effect in superconducting $[\mathrm{BaCuO}_{2+x}]_2/[\mathrm{CaCuO}_2]_3$ superlattices grown on (nominally well oriented) (001) SrTiO_3 (STO) substrates.[19]

The surface morphology of vicinal substrates can be described in terms of the arrangement of atomic steps on the surface. For example, a vicinal (001) STO surface typically consists of terraces of (001) crystal faces separated by atomic steps that accommodate the misorientation. During prolonged annealing in an oxygen atmosphere, single-atomic-height steps can aggregate to form bunches on the surface, separated by large terraces of the (001) face.[20,21] These step bunches can eventually form (100) and (010) faces. Thermal roughening and/or faceting has not been observed on the STO(001) face but on the STO (110) surface.[20] Such faceting transitions have been extensively studied for both semiconductor and metal surfaces and interfaces,[22,23] and the role of surface step structure in the formation of nanostructures is well understood,[24,25] e.g., for cases such as fractional layer superlattices (SL's).[26]

In the case of SL's based on III–V compounds, reciprocal-space mapping by x-ray diffraction was successfully used to investigate how the growth process can be controlled by the miscut of the substrate.[27–31] Moreover, such measurements were employed to study the correlation between the miscut of STO substrates and the microstructure of $\mathrm{YBa}_2\mathrm{Cu}_3\mathrm{O}_{7-\delta}$ (YBCO) thin films.[32,33]

Here we employ x-ray-diffraction and diffuse scattering measurements, using synchrotron radiation from a undulator source, to study the effect of the substrate miscut angle on the structure of the $[BaCuO_{2+x}]_2/[CaCuO_2]_3$ superlattices. These superlattices, when optimally doped, show interesting superconducting properties, such as a zero-resistance critical temperature $T_{c,0}>80$ K, a critical current density $j_c(T=0\text{ K})\approx 10^7$ A/cm^2, and a quite low in-plane anisotropy.[34] Furthermore in Ref. 35 it was shown that *in situ* reflection high energy electron diffraction (RHEED) exhibits reproducible intensity oscillations, during the growth of not superconducting $BaCuO_2/CaCuO_2$ SL's, which is a demonstration of two-dimensional growth mechanism even for superlattices of such complex oxides. With this article we provide further insight into the growth mode and the strain relief process for $[BaCuO_{2+x}]_2/[CaCuO_2]_3$ superlattices on STO substrates with different vicinal orientations. The knowledge of the nanostructure and microstructure of these superlattices is crucial in order to understand their electronic transport properties.

The superlattices were grown under the conditions specifically optimized for the best structural properties. We used substrates with carefully chosen miscut parameters, which were experimentally confirmed. The high brilliance of x rays from a third, generation synchrotron source allows us to observe the very weak diffuse intensity features coming from the interfaces structures. The experimental data obtained for the investigated samples reveal different interface morphologies, suggesting a transition from an isotropic ripple via an anisotropic ripple to a fractal structure upon increasing the miscut of the substrate. Moreover, upon enhancing the high surface sensitivity with the grazing-incidence configuration, we were able to distinguish faint asymmetrical Bragg peaks associated with different domains in the very thin layers of $[BaCuO_{2+x}]_2/[CaCuO_2]_3$ superlattices. In this way we were able to observe that the relaxation from the tetragonal to the orthorombic phase, in contrast to the structural parent high-temperature superconducting compounds, does not simply scale with the film thickness but depends strongly on the value of the miscut angle.

II. EXPERIMENTAL DETAILS

Diffraction experiments were carried out at the ID32 beamline at the European Synchrotron Radiation Facility in Grenoble. The incoming x-ray beam from two undulators was monochromatized with a Si(111) double-crystal monochromator, with the first crystal cryogenically cooled and the second crystal which provides sagittally focused, selecting an energy of 18 keV. The incident beam was defined by slits of 0.5×0.5-mm^2 size, and the momentum resolution was determined by slits of 0.5×0.5-mm^2 size in front of the detector, at a distance of 75 cm from the sample, leading to an oblique resolution element in reciprocal space with a maximum in-plane and out-of-plane projection of less than 0.06 nm^{-1}.

The deposition of *c axis-oriented* $[BaCuO_{2+x}]_2/[CaCuO_2]_3$ superlattices on STO substrates were performed using a KrF excimer laser, as already described in detail previously.[36] Prior to the deposition, the substrate was prepared by chemical etching following the procedure reported in Ref. 37, and annealed in an oxygen atmosphere for one hour at 700 °C. This produces a clean surface, mainly TiO_2 terminated,[37] providing a well-defined surface for the growth of superlattices.[38]

For the present investigation, superlattices were deposited at relatively low molecular oxygen pressure ($\leqslant 0.2$ mbar) compared with the oxygen pressure usually employed for optimum superconducting properties (≈ 1 mbar).[36] Under these conditions the superlattices are not superconducting. However the plasma plume, which depends on quite a number of not so easy to control parameters (target surface quality, laser fluence, laser spot focalization, . . .), is by far more stable, resulting in a much better control of the structural properties and higher reproducibilty from sample to sample.

$[BaCuO_{2+x}]_2/[CaCuO_2]_3$ superlattices were deposited on specially prepared miscut STO (001) substrates,[39] with the surface normal principally tilted toward the [010] direction. This was verified measuring the (002) substrate reflection for different azimuthal angles[40] both for the film and the substrate.

After alignment of the sample surface, the primitive vectors of reciprocal space were defined with respect to the lattice parameters of the STO substrate ($a=b=c=3.905$ Å) and all the *HKL* data, given in reciprocal-lattice units (r.l.u.), were normalized relative to these lattice parameters.

In order to investigate the periodicity and structural features of the superlattices in the direction normal to surface, i.e., along the [001] direction of the substrate, (001) and (002) reciprocal-space mapping in symmetrical configuration was performed in two orthogonal azimuthal directions, precisely along the in-plane [100] and [010] directions, with the crystallographic directions defined by the substrate lattice. Furthermore, to determine the interface morphology, the diffuse scattering was measured by transversal and longitudinal scans through the average lattice peak SL_0 [zeroth-order (00L) peak] and the first satellite peaks $SL_{\pm 1}$. Indeed, H and K scans (transversal scans) were performed to determine the in-plane correlation properties, and L scans (longitudinal scans) were performed to obtain the out-of-plane correlation properties.

Reciprocal-space mapping in grazing-incidence configuration around (02L) and (20L) reflections with $L=1,2$ was then performed to study the influence of the vicinality of the substrate on the strain relief process of the superlattices under investigation. During these measurements, the incidence angle of the x rays with the surface was kept constant at 0.2°, i.e., slightly higher than the critical angle. The low incidence angle was selected in order to enhance the scattering contribution from the film relative to the substrate. In this way, in-plane crystallographic reflections could be easily measured.

III. RESULTS

A. Symmetrical diffraction measurements

X-ray diffraction in a symmetrical configuration was first used to measure the vicinality of the lattice of our samples with the optical surface defined by using a laser beam. The vicinality degree was defined by the angle which the surface

TABLE I. Number of periods N of the investigated samples and vicinal angles of the surface of substrates and thin films: α_{STO} and α_{SL} are the angles between the surface normal and the [001] crystallographic directions, Φ_{STO} and Φ_{SL} are the azimuthal angles in the (001) plane measured with respect to the [010] direction.

		STO vicinal angles		SL vicinal angles	
Sample	N	α_{STO} ($\pm 0.005°$)	Φ_{STO} ($\pm 0.005°$)	α_{SL} ($\pm 0.005°$)	Φ_{SL} ($\pm 0.005°$)
1	30	0.154°	28.567°	0.146°	29.715°
2	25	0.690°	0.053°	0.702°	3.000°
3	15	0.928°	4.358°	0.854°	4.557°

normal forms with the [001] crystallographic direction (α_{STO} for STO and α_{SL} for SL's), while the vicinality direction was defined by the angle between the projection in the (001) plane of the surface normal and the [010] direction (named Φ_{STO} for STO and Φ_{SL} for SL's). These values were obtained by measuring the angular positions of the (002) Bragg reflection as a function of the azimuthal rotation of the sample surface.[40] The vicinal angles are reported in Table I. Slight differences between Φ_{STO} and Φ_{SL} for sample No. 2 and between α_{STO} and α_{SL} for sample No. 3 can be observed. These different vicinal angles can be explained by considering misfit dislocations at the STO/SL interface. Indeed, the in-plane lattice mismatch (-1.1% for $\mathrm{CaCuO_2}$ and larger than 0.5% for $\mathrm{BaCuO_{2+x}}$ relative to the STO substrate) is accommodated in the first layers by an elastic distortion of the crystallographic cell. Increasing the thickness, the next layers relax the accumulated strain by a dislocation network. The miscut favors dislocations with components of the Burgers vector parallel to the interface and, therefore, misorientations between STO and SL planes can arise. This effect was already observed in $\mathrm{SrCuO_2/CaCuO_2}$ SL's.[41] Moreover, no significant discrepancies in the vicinal angles between the substrate and SL appear in the case of sample No. 1, due to the very low miscut angle.

K-L reciprocal-space maps in symmetrical configuration are reported in Fig. 1 for the three samples. In these maps the in-plane scattering vector is along the [010] crystallographic direction (the principal miscut direction). *H-L* maps recorded with the in-plane scattering vector rotated by 90° (along the [100] direction) are shown in Fig. 2.

The *K-L* maps of Fig. 1 show that the crystal truncation rods (CTR's) from the (001) and (002) reflections, indicated by straight white lines in the maps, do not coincide, and their distance ΔK increases with the miscut angle of the substrate, as expected. No splitting of the CTR's is observed in the maps of Fig. 2. These results are a signature of the very regular alignment of the step arrays along the miscut direction for all the investigated samples.

In both Figs. 1 and 2 we can see that the diffusely scattered intensity is concentrated into periodic sheets perpendicular to the out-of-plane scattering vector (L direction). This feature indicates that the interface profiles are strongly replicated in the growth direction.[42]

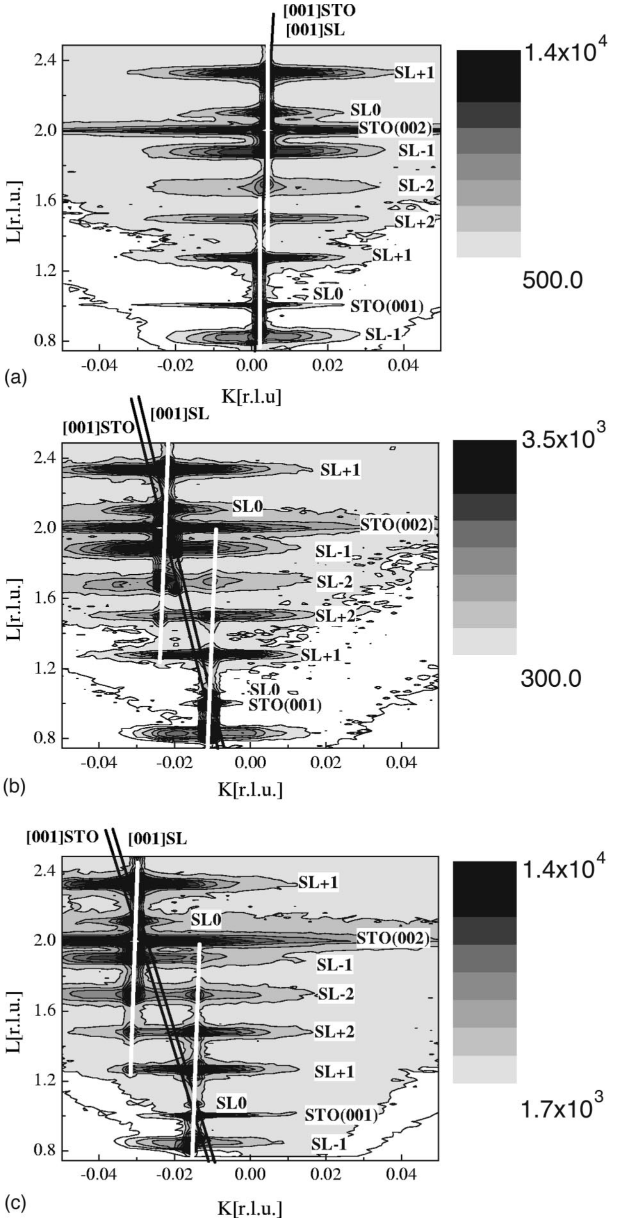

FIG. 1. Isointensity contour plot on a logarithmic scale of the (001) and (002) reciprocal-space maps in a symmetrical configuration with the samples oriented along the principal miscut direction [010]. The three samples are grown on STO substrates with different miscut angles: (a) sample No. 1, (b) sample No. 2, and (c) sample No. 3. The black straight lines are along the [001] crystallographic directions, and the white straight lines highlight the (001) and (002) CTRs.

In Fig. 1 the [001] crystallographic directions of the substrate and the SL's are indicated by straight black lines. From the difference between the out-of-plane scattering vector $Q_\perp$ at the first-order satellite peaks (SL_{-1} and SL_{+1}) it is possible to obtain a rough estimation of the vertical periodicity Λ of the superlattice by

$$\Lambda = \frac{4\pi}{|Q_\perp(SL_{+1}) - Q_\perp(SL_{-1})|}$$

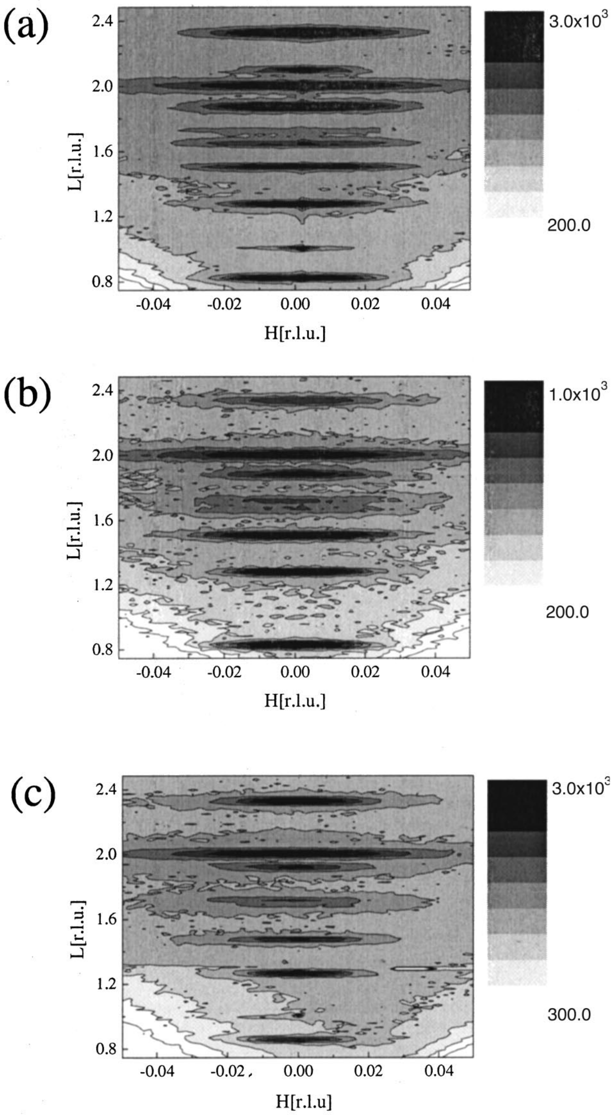

FIG. 2. Isointensity contour plot on a logarithmic scale of the (001) and (002) reciprocal-space maps in a symmetrical configuration with the samples oriented along the in-plane crystallographic direction [100]. The three samples are the same as in Fig. 1.

where $Q_\perp(SL_{+1})$ and $Q_\perp(SL_{-1})$ represent the $Q_\perp$ values of the first-order satellite peaks. The values of Λ are reported in Table II, together with the perpendicular average lattice parameter of the SL's, $\overline{c}_{\mathrm{SL}}=2\pi/\Delta Q_\perp(SL_0)$, where $\Delta Q_\perp(SL_0)$ is the difference between the $Q_\perp$ values of the zeroth-order $SL_0(001)$ and $SL_0(002)$ peaks.

TABLE II. Out-of-plane crystallographic characteristics extracted by symmetrical scans: $\overline{c}_{\mathrm{SL}}$ is the average lattice parameter and Λ is the periodicity obtained as described in the text.

Sample	$\overline{c}_{\mathrm{SL}}$ (Å)	Λ (A)
1	3.744 ± 0.002	17.39 ± 0.12
2	3.724 ± 0.002	17.53 ± 0.12
3	3.705 ± 0.002	18.03 ± 0.18

B. Diffuse scattering

Vicinality can give rise to asymmetrical in-plane and out-of-plane coherence lengths, which can be investigated by measuring the diffuse scattering in transversal and longitudinal scans, respectively, at different azimuthal directions. When the distribution of the diffusely scattered intensity exhibits lateral shoulders, theoretical calculations and experiments demonstrate (see, for example, Refs. 43–45) that the interface structure can be described by a sequence of self-similar motives, called ripples. A particular case is given by a regular alignment of steps. The spacing between the shoulders is inversely proportional to the real-space separation between the ripples and eventually to the mean width of terraces and steps.[46] The absence of pronounced shoulders is due to the dispersion of the statistical distribution of the ripple width, and it can be explained using a conventional fractal model of the interface roughness.[47]

Transversal scans through several superstructure peaks were carried out for two orthogonal azimuthal directions for each sample, to obtain information about the correlation between the interface morphology and the miscut direction. Measurements of the first-order satellite peak SL_{-1} of the (002) reflection are shown in Fig. 3. Lateral shoulders are clearly visible in the diffuse scattering of samples Nos. 1 and 2, indicating a ripple structure with a characteristic lateral length. They disappear in the case of sample No. 3, where the miscut is even larger.

The diffuse scattering of sample No. 1, having the lowest miscut angle, shows symmetrical shoulders in both the [010] and [100] crystallographic directions [see Fig. 3(a)], which can be assigned to a symmetric ripple structure at the interface in both the crystallographic directions. Due to the sharpness of the lateral shoulders, we can estimate the average distance $l_\parallel$ between the ripples from $l_\parallel\approx4\pi/\delta Q_\parallel$, where $\delta Q_\parallel$ is the separation between lateral shoulders[46] in Å^{-1} units ($Q_\parallel$ is the in-plane scattering vector). The values of $l_\parallel$, reported in Table III, are almost independent from the azimuthal angle, in agreement with a circular shape of islands, as already reported in the literature for the growth of perovskite oxide materials (see, for example Ref. 48).

Conversely, asymmetrical shoulders are observed in the diffuse scattering of sample No. 2 along the [010] crystallographic direction [see Fig. 3(b)]. However, the shoulders disappear when the sample is azimuthally rotated by 90° (i.e., along the [100] direction). The asymmetry of the shoulders is due to the asymmetry of the shape of the ripples, which are elongated along the [010] crystallographic direction (the principal miscut direction). The presence of unidirectional ripples can be attributed to a stepped interface. In this framework the values of $l_\parallel$, reported in Table III for the [010] direction, can be regarded as the step sizes. For the [100] direction, where no lateral shoulders are observed, the average coherence lengths is estimated by 2π/FWHM, where FWHM is the full width at half maximum of the peaks in Å^{-1} units. The additional lateral peak observed in the K scan of Fig. 3(b) has a completely different origin. It arises from the CTR of the (001) reflection of the STO.

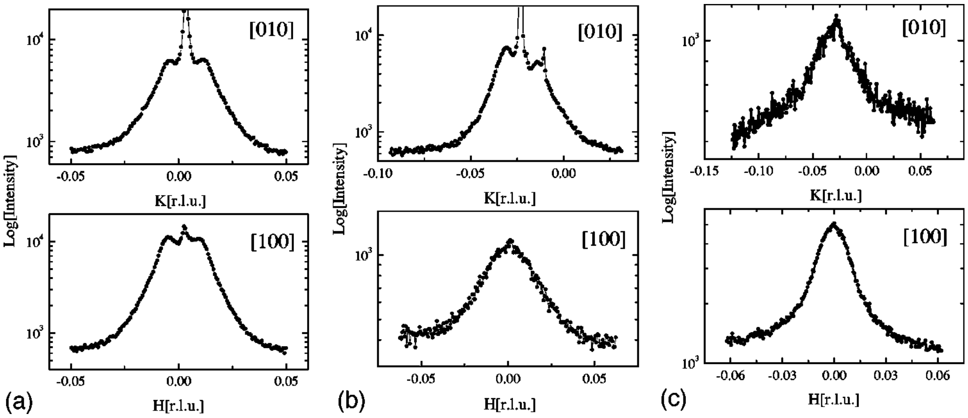

FIG. 3. Diffuse scattering measured by transversal scans through the first-order satellites SL_{-1} of the (002) reflection of the three samples grown on STO with different miscut angles: (a) sample No. 1, (b) sample No. 2, and (c) sample No. 3. For all samples the scans were performed along the two orthogonal in-plane crystallographic directions [010] (top graphs) and [100] (bottom graphs).

With further increasing of the miscut angle no lateral shoulders can be observed in the case of sample No. 3 [see Fig. 3(c)]. This can be explained by assuming that ripples exhibit a very large dispersion of their widths. Thus it may be more appropriate to describe this by a fractal structure at the interface.[49] For this sample the in-plane coherence lengths reported in Table III are deduced by the FWHM (in Å^{-1} units) of the transversal scans, and they are not related to the ripple sizes at the interface.

In Table III the approximate terrace widths of the STO, which are calculated assuming monolayer high steps, are also reported. Furthermore, longitudinal scans of sample No. 1 in both the [010] and [100] crystallographic directions, and of sample No. 2 along the [010] direction, clearly showed size effects. In these cases the out-of-plane coherence lengths $l_\perp$ can be regarded as the coherent thicknesses, obtained by the size simulation using

$$I = I_0 \left[\frac{\sin(tQ_\perp/2)}{\sin(dQ_\perp/2)} \right]^2,$$

where I_0 represents a scale factor, t the coherent thickness, and d the lattice spacing. This equation is based on the assumption of the existence of crystalline coherence in the film, without any surface and interface roughness. Therefore, the agreement between theoretical and experimental data is only approximate. An L scan through the first-order satellite SL_{+1} of sample No. 2 is shown in Fig. 4, where the very pronounced size effect can be observed. However, in longitudinal scans of sample No. 2 along the [100] direction and of sample No. 1 in both the [010] and [100] crystallographic directions, size effects are not present. In these cases the out-of-plane coherence lengths $l_\perp$ are obtained from the FWHM in Å^{-1} units of the longitudinal scans by 2π/FWHM. $l_\perp$ values are reported in Table IV.

TABLE III. Average values of the in-plane coherence lengths $l_\parallel$ obtained by 2π/FWHM, where the FWHM is the full width at half maximum in Å^{-1} units of the *transversal* scans through several reflections of SL's. The values indicated with * are calculated by $4\pi/\delta Q_\parallel$, where $\delta Q_\parallel$ is the difference between the in-plane scattering vector values at the lateral shoulders. l_{STO} is the approximate size of the steps of the substrate calculated assuming monolayer height steps by $a/\tan(\alpha_{\text{STO}})$ where α_{STO} is the miscut angle and a is the lattice constant of the STO.

Sample	$l_\parallel$ (Å) [010]	$l_\parallel$ (Å) [010]	l_{STO} (Å)
1	465±10*	449±10*	1450
2	144±5	161±5*	324
3	186±10	88±5	241

C. Grazing-incidence diffraction measurements

Grazing-incidence diffraction (GID) is a valuable tool for studying in-plane structural properties of epitaxial thin films. With a sufficiently small angle of incidence, this diffraction geometry allows us to obtain information mainly associated with the thin overlayer and in particular with its in-plane properties because of the very small vertical component of the scattering vector.

We collected several maps in GID configuration to investigate the in-plane structure in detail and to determine the a_{SL} and b_{SL} lattice parameters of the SL. We performed *H-K* mapping for each sample around four reflections, i.e., around the [021], [022], [201], and [202] reciprocal-lattice points of the SL's. The in-plane lattice parameters were then calculated by $a_{\text{SL}} = aH(\text{STO})/H(\text{SL})$ and $b_{\text{SL}} = bK(\text{STO})/K(\text{SL})$, i.e., by the ratio of the H and K values in r.l.u. of the STO and SL reflections. The results are reported in Table V. It can be

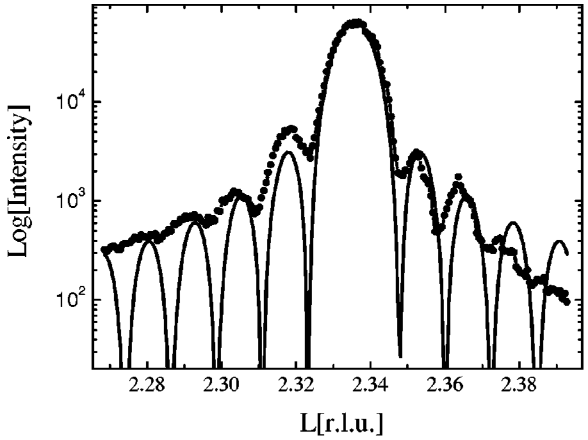

FIG. 4. Longitudinal scan through the SL_{+1} satellite of the (002) reflection of sample No. 2 where the size effect can be clearly observed: experimental data (dotted line) and simulation (continuous line) are as described in the text.

TABLE IV. Average values of the out-of-plane coherence lengths $l_\perp$ obtained by 2π/FWHM where FWHM is the full width at half maximum in Å^{-1} units of the *longitudinal* scans through several reflections of SL's. The values indicated with * correspond to the coherent thickness obtained by simulation of the size effect.

Sample	$l_\perp$ (Å) [100]	$l_\perp$ (Å) [010]
1	274±5*	300±5*
2	122±5	318±5*
3	205±10	80±5

observed that the miscut angle of the substrate strongly influences the in-plane lattice constants of the film. Larger miscut angles, and thus the presence of steps with shorter terraces on the substrate, reduce the film strain by a transition from its lattice-matched, tetragonal structure to an orthorhombic phase.

Sample No. 1, having a lower miscut angle, is perfectly tetragonal and fully strained, as demonstrated by the lattice parameters shown in Table V. However, in the case of sample No. 2, having the intermediate miscut angle, we can detect the presence of different domains. Indeed the (022) and (202) maps reported in Fig. 5 show four different peaks: two more intense, $P1$ and $P2$, and two weaker, $P3$ and $P4$. The stronger peaks $P1$ and $P2$ correspond to an orthorhombic structure with the a_{SL} and b_{SL} in-plane axes aligned along the in-plane crystallographic directions of the substrate. The two peaks are due to the scattering from two sets of crystallographic planes characterized by the exchange of the directions of the a_{SL} and b_{SL} axis of the film. This provides clear evidence of twinning as a result of the lattice relaxation of the film beyond the critical thickness for pseudomorphic growth, which, in turn, appears to be influenced by the miscut of the substrate. The sketch of the in-plane cell of the film on the substrate for the orthorhombic domain is shown in Fig. 6(a) in the case of the a_{SL} axis perpendicular to the step edge. The lattice parameters of the orthorhombic structure reported in Table V are calculated by using the positions of the peaks $P1$ and $P2$. However, the weaker peaks $P3$ and $P4$ can be tentatively associated with another kind of domain in which the structure is tetragonal, but with a slight rotation of the axes of the film with respect to those of the substrate, which is illustrated by the sketch in Fig. 6(b). The peak positions of $P3$ and $P4$ give the value of the tetragonal lattice parameter, which is almost equal to the average between a_{SL} and b_{SL} of the orthorhombic structure, practically equal to the lattice parameter of STO. From the map around the (202) reflection [see Fig. 5(b)] in which the $P3$ and $P4$ peaks are more intense, the rotation of the tetragonal cell of the film has been calculated by arctan $(\Delta K_{P3,P4}/H_{\mathrm{center}})$. This gives 0.042°. In this formula $\Delta K_{P3,P4}$ is the difference between the K values of the $P3$ and $P4$ peaks and H_{center} is the H value in the center between the peaks.

TABLE V. In-plane lattice parameters measured by grazing-incidence diffraction and the calculated in-plane area of the crystallographic cell of the SL's.

Sample	a_{SL} (Å)	b_{SL} (Å)	In-plane area (Å^2)
1	3.903±0.002	3.905±0.001	15.24±0.01
2	3.889±0.001	3.929±0.001	15.28±0.01
3	3.898±0.002	3.920±0.001	15.28±0.01

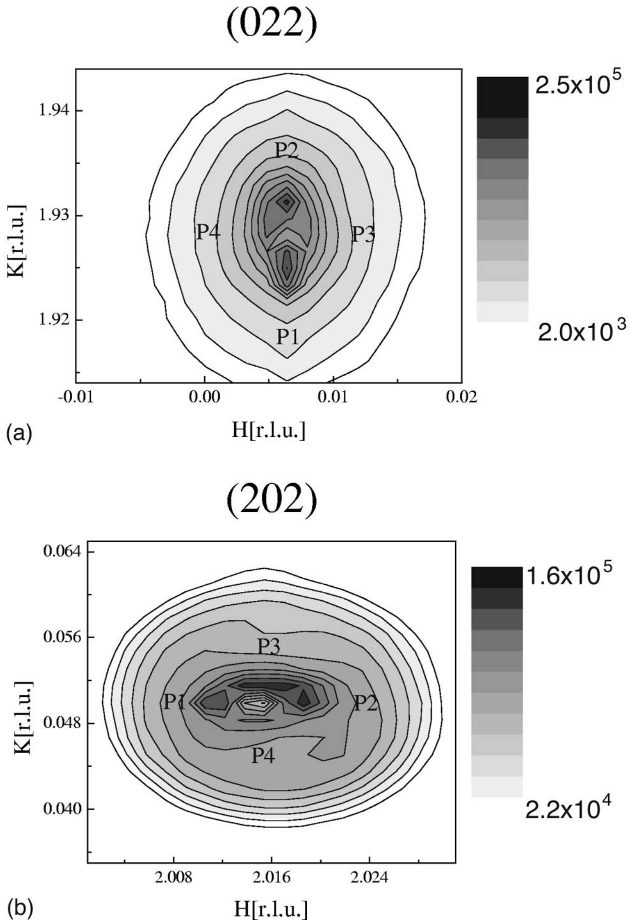

FIG. 5. Isointensity contour plot on a logarithmic scale of reciprocal-space maps in grazing-incidence configurations for sample No. 2 around the (022) (a) and (202) (b) reflections of the SL.

Moreover, for sample No. 3, having the largest miscut angle, we observe that the structure is orthorhombic with no tetragonal domains. Values of the in-plane axes are reported in Table V. No twin domains are observed: the shorter axis (indicated as a_{SL}) is aligned normal to the step edges, as shown in Fig. 6(a). The same observation was previously made for the growth of YBCO on STO(001), where the longer b axis was found to be aligned with the step edges and the shorter axis was aligned normal to the step edges, with the result of an almost twin-free film.[33] The driving force responsible for the alignment of the axes is probably associated with a slight compressibility of the terraces normal to the step edges, thus accommodating the shorter axis of the film more easily, as discussed earlier.[33] The alignment of the film axes may also be associated with different values of surface energy of the step edge at the interface between film

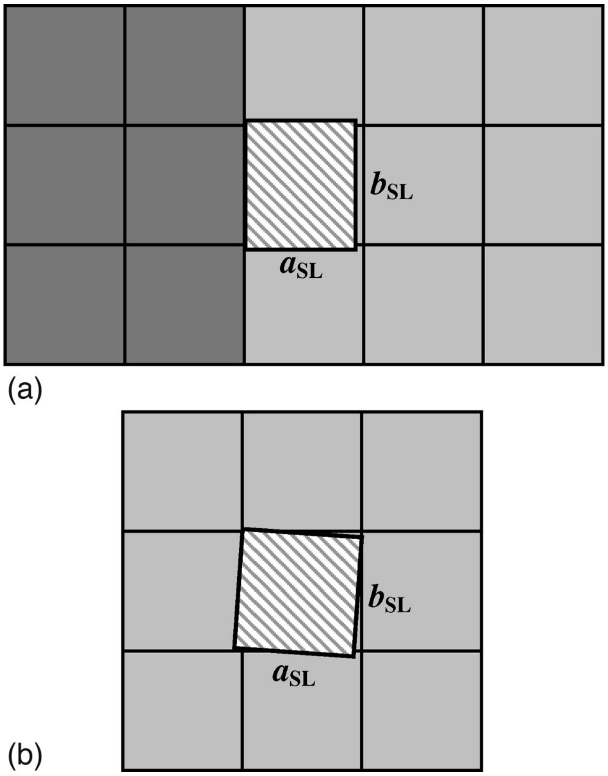

FIG. 6. Top view of the in-plane lattice of the substrate and the film in real space. In (a) the gray squares are the STO cells and the different gray levels correspond to different heights of the terraces: dark gray cells are one unit cell higher than the light gray cells. At the edge of the terrace the orthorombic cell of the SL (hatched rectangle) is oriented with the a_{SL} axis perpendicular to the step edge. In (b) the in-plane lattice square of the STO (without considering different terraces) and the slightly rotated tetragonal cell of the SL are shown. The rotation of the cell is notably magnified with respect to the obtained value of 0.042°.

and substrate. The tetragonal-orthorhombic transition, induced by the asymmetry of the substrate with increasing miscut angle, is accompanied by a slight increase of the in-plane unit cell area relative to that of the substrate (15.25 Å^2), as reported in Table V.

IV. DISCUSSION

Two parameters influence the crystallographic structure and the morphology of the investigated samples: thickness and miscut angle.

A. Crystallographic structure

In HTS thin films, when the bulk structure of the material is orthorhombic (for example in YBCO), a tetragonal-orthorhombic transition is observed when the film thickness is larger than a critical value.[50] An opposite trend is observed in our samples: grazing-incidence diffraction measurements showed a tetragonal-orthorhombic transition in thinner films driven by the misorientation of the substrate. Moreover the thickness can be responsible for the development of a dislocation network at the interface between the SL and the STO.

In the case of a very low miscut angle, sample No. 1 ($\alpha_{SL} \approx 0.15°$ and $N=30$), which is the thickest of the three samples, is still not thick enough to relax the strain, since the in-plane lattice constants of film and substrate are the same within the error, in agreement with a coherent epitaxial growth of this SL. When the miscut is larger (see sample Nos. 2 and 3) the SL's tend to become orthorhombic, even if the difference between the a_{SL} and b_{SL} lattice parameters is very small. In sample No. 3 ($\alpha_{SL} \approx 0.85°$ and $N=15$) the cell is orthorhombic without any indication of twin domains, which means that the critical thickness is not yet reached. Sample No. 2 ($\alpha_{SL} \approx 0.70°$ and $N=25$), despite being thinner than sample No. 1, the thickness exceeds the critical value for pseudomorphic and untwinned growth due to the higher miscut angle. Therefore, a network of misfit dislocations occurs to relax the strain. This is confirmed by the difference in Φ angle values between the film and substrate, i.e., the slight rotation of in-plane vicinality direction, and the presence of different domains.

The elastic distortion of the SL crystallographic structure can be seen from the values of the lattice parameters reported in Tables II and V. The in-plane unit cell increases together with a decrease of the $\overline{a}_{SL}$ axis.

Furthermore, in the case of the twin-free, orthorhombic SL (sample No. 3) the alignment of the shorter a_{SL} axis perpendicular to the step edge [see Fig. 6(a)] will be stimulated by the attempt of the film to minimize the interface energy. This is suggested to be the general thermodynamic driving force inducing the alignment during the growth process of HTS film.[51]

B. Interface morphology

The results of the diffuse scattering measurements allowed us to study the interface ordering. A very regular alignment of the step arrays along the miscut direction for all the investigated samples was deduced from the symmetrical reciprocal space maps, where the $(00L)$ CTR's from both (001) and (002) reflections split the superlattice reflections into two peaks separated by ΔK values proportional to the tilt. A different ordering of steps could be deduced from the results of the diffuse scattering measurements. The small miscut angle of $\alpha_{SL} \approx 0.70°$ in sample No. 2 is enough to induce a higher degree of ordering in the steps distribution. The absolute value of the step size in sample No. 2 is smaller relative to sample No. 1 ($\alpha_{SL} \approx 0.15°$). However, comparing the coherence length $l_{\parallel}$ with the dimension l_{STO} of the terraces of the substrate (Table III), sample No. 2 appears to be, on average, more ordered. Further increasing the misorientation, the disorder increases and when the miscut angle is about 0.85° (sample No. 3), disorder in the spacing of the steps gives rise to a broadening of the two CTR's.

The presence of ripples at interfaces of SL's with lower miscut angles, sample No. 1 with $\alpha_{SL} \approx 0.15°$ and sample No. 2 with $\alpha_{SL} \approx 0.70°$, indicate a layer-by-layer growth mode. This is in agreement with previous RHEED studies performed on these superlattices.[35] In particular, in the case of sample No. 1, the symmetry of the ripples and its invariance under 90° rotation, indicate an isotropic interface structure. This can be associated to a two-dimensional (2D) growth mode with coalescence of isotropic, two-dimensional islands or to some tendency towards 2D/3D Stranski-Krastanov growth, induced by occasional defects during the growth process. This isotropy can be attributed to the combination of the lowest miscut angle and the largest thickness of the sample and is in agreement with scanning tunneling microscopy studies of YBCO thin films on STO substrates.[52] However, in the case of sample No. 3 no ripples are present, and the larger miscut angle introduces a high degree of interface disorder.

The relaxation of the stress, which is induced by the inplane lattice mismatch, was proposed to be one of the reasons for the transition from a 2D to a 3D growth mode in YBCO films grown by various techniques, but other mechanisms were also proposed to explain this phenomenon.[53,54] In the case of SL's the strain may be responsible for the 3D growth mode, while the vicinality is responsible for the improvement of the interface quality only for low miscut angles. No ordered steps and low coherence lengths are observed for the miscut angle of almost 0.85°, and step bunching is not observed. These values of the misorientation are quite small in comparison with results reported in the literature on III–V compounds superlattices, where macrosteps are observed at larger miscut angles.[28]

V. CONCLUSION

In summary, in the present study we investigated structural and morphological properties of $[\mathrm{BaCuO}_{2+x}]_2/[\mathrm{CaCuO}_2]_3$ superlattices grown by pulsed-laser deposition on vicinal (001) SrTiO_3 substrates with different miscut values. X-ray-diffraction and diffuse scattering measurements, both in conventional and in grazing-incidence geometries provided detailed information about the role of the miscut on structure and morphology of the films. During the growth process even a small miscut of the substrate influences the orientation and the isotropy of the ripples at the interface. Three types of interface structure have been observed as a function of miscut angle below 1°, namely, a symmetric ripple structure for the smallest angle, an asymmetric ripple structure for the intermediate angle, and an isotropic fractal structure for the largest misorientation. The results have shown that a miscut angle of about 0.70° improves the ordering at the interfaces of $[\mathrm{BaCuO}_{2+x}]_2/[\mathrm{CaCuO}_2]_3$ superlattices, but a further increase leads to a worsening of the interface properties at a degree of misorientation which is much smaller than normally employed for the growth of semiconductor superlattices. The tetragonal-to-orthorhombic transition is also favored by the vicinality of the substrate, and depends less on the thickness of the films. Therefore, defining a unique value for the critical thickness for the strain relaxation, which is accompanied by the tetragonal-to-orthorhombic transition, as in the case of other HTS's thin films, is questionable in the case of $[\mathrm{BaCuO}_{2+x}]_2/[\mathrm{CaCuO}_2]_3$ superlattices. However, a larger thickness may favor the transition from the 2D to 3D growth mode, as already observed in other HTS's thin films. To the best of our knowledge this is the first study of the effect of the miscut angle in the growth mode of artificial superlattices with a such complex oxide structure. Since rather small miscut angles already strongly influence the morphology and structure of these superlattices, the knowledge and choice of the miscut of the substrate is crucial in order to grow $[\mathrm{BaCuO}_{2+x}]_2/[\mathrm{CaCuO}_2]_3$ superlattices with well-defined structural properties.

ACKNOWLEDGMENT

The authors would like to thank the staff of the ID32 beamline at the ESRF for the technical assistance during the experiment.

---

*Electronic mail: aruta@na.infn.it

†Present address: Pirelli Labs, Viale Sarca 222, 20126 Milano, Italy.

[1] G. Balestrino, S. Martellucci, P. G. Medaglia, A. Paoletti, G. Petrocelli, and A. A. Varlamov, Phys. Rev. B **58**, R8925 (1998).

[2] X. Li, T. Kawai, and S. Kawai, Jpn. J. Appl. Phys. **33**, L18 (1994).

[3] H.-U. Habermeier, G. Cristiani, R. K. Kremer, O. Lebedev, and G. van Tendeloo, Physica C **298**, 364 (2001).

[4] H. Tanaka, N. Okawa, and T. Kawai, Solid State Commun. **110**, 191 (1999).

[5] K. Ueda, H. Saeki, H. Tabata, and T. Kawai, Solid State Commun. **116**, 221 (2000).

[6] P. A. Salvador, A.-M. Haghiri-Gosnet, B. Mercey, M. Hervieu, and B. Raveau, Appl. Phys. Lett. **75**, 2638 (1999).

[7] B. D. Qu, M. Evstigneev, D. J. Johnson, and R. H. Prince, Appl. Phys. Lett. **72**, 1394 (1998).

[8] K. Iijima, T. Terashima, Y. Bando, K. Kamigaki, and H. Terauchi, J. Appl. Phys. **72**, 2840 (1992).

[9] J. Choi and C. B. Eom, G. Rijnders, H. Rogalla, and D. H. A. Blank, Appl. Phys. Lett. **79**, 1447 (2001).

[10] G. Koster, K. Verbist, G. Rijnders, H. Rogalla, G. van Tendeloo, and D. H. A. Blank, Physica C **167**, 353 (2001).

[11] S. Bals, G. Van Tendeloo, M. Salluzzo, and I. Maggio-Aprile, Appl. Phys. Lett. **79**, 3660 (2001).

[12] T. Haage, J. Zegenhagen, H.-U. Habermeier, and M. Cardona, Phys. Rev. Lett. **80**, 4225 (1998).

[13] J. Kim, D. B. Chrisey, J. S. Horwitz, M. M. Miller, and C. M. Gilmore, J. Mater. Res. **15**, 596 (2000).

[14] J.-C. Nie, H. Takashima, N. Terada, A. Shoji, and M. Koyanagi, Jpn. J. Appl. Phys., Part 2 **38**, L1499 (1999).

[15] T. Haage, J. Zegenhagen, J. Q. Li, H.-U. Habermeier, M. Cardona, Ch. Jooss, R. Warthmann, A. Forkl, and H. Kronmüller, Phys. Rev. B **56**, 8404 (1997).

[16] Ch. Jooss, R. Warthmann, and H. Kronmüller, Phys. Rev. B **61**, 12433 (2000).

[17] J. H. Durrell, G. Gibson, Z. H. Barber, J. E. Evetts, R. Rössler, J. D. Pedarnig, and D. Bäuerle, Appl. Phys. Lett. **77**, 1686 (2000).

[18] Y. Z. Zhang, R. Deltour, J.-F. de Marneffe, Y. L. Qin, L. Li, Z. X. Zhao, A. G. M. Jansen, and P. Wyder, Phys. Rev. B **61**, 8675 (2000).

[19] C. Aruta, J. Zegenhagen, B. Cowie, G. Balestrino, G. Pasquini, P. G. Medaglia, F. Ricci, D. Luebbert, T. Baumbach, E. Riedo, L.

Ortega, R. Kremer, and J. Albrecht, Phys. Status Solidi A **183**, 353 (2001).

[20] Q. D. Jiang and J. Zegenhagen, Surf. Sci. **367**, L42 (1996).

[21] J. Zegenhagen, T. Haage, and Q. D. Jiang, Appl. Phys. A: Mater. Sci. Process. **67**, 711 (1998).

[22] M. V. Ramana Murthy, P. Fini, G. B. Stephenson, C. Thompson, J. A. Eastman, A. Munkholm, O. Auciello, R. Jothilingam, S. P. DenBaars, and J. S. Speck, Phys. Rev. B **62**, R10661 (2000).

[23] S. Brennan, G. B. Stephenson, P. H. Fuoss, D. W. Kisker, C. Lavoie, and K. L. Evans-Lutterodt, J. Appl. Phys. **88**, 3367 (2000).

[24] F. Liu, J. Tersoff, and M. G. Lagally, Phys. Rev. Lett. **80**, 1268 (1998).

[25] J.-M. Baribeau, D. J. Lockwood, and R. W. G. Syme, J. Appl. Phys. **80**, 1450 (1996).

[26] T. Fukui and H. Saito, J. Vac. Sci. Technol. B **6**, 1373 (1988).

[27] C. Giannini, T. Baumbach, D. Lüebbert, R. Felici, L. Tapfer, T. Marschner, W. Stolz, N. Y. Jin-Phillipp, and F. Phillip, Phys. Rev. B **61**, 2173 (2000).

[28] C. Giannini, L. Tapfer, Y. Zhuang, L. DeCaro, T. Marschner, and W. Stolz, Phys. Rev. B **55**, 5276 (1997).

[29] M. Schimdbauer, R. Opitz, Th. Wiebach, and R. Kohler, Phys. Rev. B **64**, 195316 (2001).

[30] R. S. Goldman, K. L. Kavanagh, H. H. Wieder, S. N. Ehrlich, and R. M. Feenstra, J. Appl. Phys. **83**, 5137 (1998).

[31] J. A. Olsen, E. L. Hu, and S. R. Lee, J. Appl. Phys. **79**, 3578 (1996).

[32] J. Brötz, H. Fuess, T. Haage, J. Zegenhagen, Ch. Jooss, A. Forkl, and R. Warthmann, J. Appl. Phys. **85**, 635 (1999).

[33] J. Brötz, T. Haage, J. Zegenhagen, and H. Fuess, Phys. Rev. B **57**, 3679 (1998).

[34] G. Balestrino, S. Lavanga, P. G. Medaglia, S. Martellucci, A. Paoletti, G. Pasquini, G. Petrocelli, A. Tebano, A. A. Varlamov, L. Maritato, and M. Salvato, Phys. Rev. B **62**, 9835 (2000).

[35] A. Tebano, G. Balestrino, S. Lavanga, S. Martellucci, P. G. Medaglia, A. Paoletti, G. Pasquini, G. Petrocelli, and A. Tucciarone, Physica C **355**, 335 (2001).

[36] G. Balestrino, G. Martellucci, P. G. Medaglia, A. Paoletti, and G. Petrocelli, Physica C **302**, 78 (1998).

[37] M. Kawasaki, K. Takahashi, T. Maeda, R. Tsuchiya, M. Shinohara, O. Ishiyama, T. Yonezawa, M. Yoshimoto, and H. Koinuma, Science **266**, 1540 (1994).

[38] G. Koster, B. L. Kropman, G. J. H. M. Rijnders, D. H. A. Blank, and H. Rogalla, Appl. Phys. Lett. **73**, 2920 (1998).

[39] CRYSTAL GmbH, Berlin, Germany

[40] P. Maigne and A. P. Roth, J. Cryst. Growth **118**, 117 (1992).

[41] A. DelVecchio, L. Tapfer, C. Aruta, G. Balestrino, and G. Petrocelli, J. Appl. Phys. **80**, 781 (1996).

[42] V. Holy and T. Baumbach, Phys. Rev. B **49**, 10 668 (1994).

[43] R. L. Headrick and J.-M. Baribeau, J. Vac. Sci. Technol. A **13**, 782 (1995).

[44] J. Tersoff, C. Teichert, and M. G. Lagally, Phys. Rev. Lett. **76**, 1675 (1996).

[45] J. Grim, V. Holy, J. Kubena, J. Stangl, A. A. Darhuber, S. Zerlauth, F. Schaffler, and G. Bauer, J. Phys. D **32**, A216 (1999).

[46] V. Holy, C. Giannini, L. Tapfer, T. Marschner, and W. Stolz, Phys. Rev. B **55**, 9960 (1997).

[47] S. K. Sinha, E. B. Sirota, S. Garoff, and H. B. Stanley, Phys. Rev. B **38**, 2297 (1989).

[48] R. A. Rao, Q. Gan, and C. B. Eom, Appl. Phys. Lett. **71**, 1171 (1997).

[49] G. Palasatzas and J. Krim, Int. J. Mod. Phys. B **9**, 599 (1995).

[50] Q. D. Jiang, D.-M. Smilgies, R. Feidenhans'l, M. Cardona, and J. Zegenhagen, Solid State Commun. **98**, 157 (1996).

[51] F. Miletto Granozio, F. Ricci, U. Scotti di Uccio, and J. C. Villagier, Phys. Rev. B **57**, 6173 (1998).

[52] X.-Y. Zheng, D. H. Lowndes, S. Zhu, J. D. Budai, and R. J. Warmack, Phys. Rev. B **45**, 7584 (1992).

[53] M. Salluzzo, C. Aruta, I. Maggio-Aprile, Ø. Fischer, J. Zegenhagen, and S. Bals, Phys. Status Solidi A **186**, 339 (2001).

[54] B. Dam, J. M. Huijbregtse, and J. H. Rector, Phys. Rev. B **65**, 064528 (2002).